A STUDY OF ELECTROCHEMICAL TRANSPORT AND DIFFUSE CHARGE DYNAMICS USING A LANGEVIN EQUATION

BY

KARTHIK CHIKMAGALUR

THESIS

Submitted in partial fulfillment of the requirements
for the degree of Master of Science in Theoretical and Applied Mechanics
in the Graduate College of the
University of Illinois at Urbana-Champaign, 2011

Urbana, Illinois

Adviser:

Professor David Saintillan

ABSTRACT

This thesis aims to develop new numerical and computational tools to study electrochemical transport and diffuse charge dynamics at small scales. Previous efforts at modeling electrokinetic phenomena at scales where the non-continuum effects become significant have included continuum models based on the Poisson-Nernst-Planck equations and atomic simulations using molecular dynamics algorithms. Neither of them is easy to use or conducive to electrokinetic transport modeling in strong confinement or over long time scales. This work introduces a new approach based on a Langevin equation for diffuse charge dynamics in nanofluidic devices, which incorporates features from both continuum and atomistic methods. The model is then extended to include steric effects resulting from finite ion size, and applied to the phenomenon of double layer charging in a symmetric binary electrolyte between parallel-plate blocking electrodes, between which a voltage is applied. Finally, the results of this approach are compared to those of the continuum model based on the Poisson-Nernst-Planck equations.

ACKNOWLEDGMENTS

The author wishes to express sincere appreciation and gratitude towards Professor Saintillan for his guidance over the period of this study. His support and patience have been invaluable. The author also thanks his parents for their constant encouragement and support. Finally, he wishes to acknowledge the academic resources made available by the university, in particular the Grainger Engineering Library for access to instructional materials on this interesting but initially unfamiliar subject.

TABLE OF CONTENTS

LIST OF SYMBOLS

λ, λ_D	Debye layer thickness
ε_0	Permittivity
ζ	Zeta-potential (Potential drop across the EDL)
μ	Viscosity
$\boldsymbol{u_s}$	Slip velocity
$\boldsymbol{u}$	Local fluid velocity
$\boldsymbol{v}_\pm$	Flux velocity
z	Valence of ion species
e	Elementary charge
$c_\pm$	Ion charge densities
ϕ	Electric potential
$\boldsymbol{n}$	Random Gaussian variable with zero mean, unit variance
k	Boltzmann's constant
T	Temperature
D	Diffusivity
a	Particle/ion radius
ψ_n	Incomplete Gamma function of order n

CHAPTER 1

INTRODUCTION

Recent advances in microfabrication technologies have enabled engineers and scientists to design and manufacture ever smaller fluidic devices to meet new engineering challenges and tackle new applications [1–3]. These new breakthroughs in manufacturing have generated much interest over the last few years owing to their potential applications in a variety of fields and specifically for the miniaturization of chemical and biological assays [4–6]. Yet more recently, efforts have focused on further scaling these devices down to the nanoscale, opening a new realm of physical phenomena [7]. The emergence of micro- and nanofluidics and of lab-on-chip technology has enabled the development of numerous novel devices achieving various functions, such as cell separation and sorting [8], chemical and biochemical separations [9], biochemical detection and analysis [10], logic gates [11,12], and many others.

These developments have brought about a wealth of new design and modeling challenges, as the physics that govern these systems differ significantly from their macroscale counterparts [1]. In particular, fluid flows in micro- and nanodevices are characterized by the complete absence of inertia, which makes them reversible and renders mixing difficult. Also, they are often dominated by interfacial effects owing to the large surface-to-volume ratio at these length scales. Thermal, electric and chemical effects are also often present and intimately coupled, leading to a broad spectrum of new phenomena for which a good theoretical understanding and accurate models are often lacking.

Of particular interest has been the use of electric fields and electrokinetic phenomena in these devices as an efficient and low-cost means for transporting fluid and manipulating particles [13] or macromolecules [14]. Most solid surfaces possess a native charge resulting from chemical reactions with the surrounding electrolyte [13, 15, 16]. These charged surfaces in turn attract ions of opposite charge in the liquid, which accumulate near the boundary

creating an electrical double layer. When subjected to an electric field, this double layer exerts a body force on the fluid near the surface, which can drive fluid or particle motion. This technique for manipulating fluid and particles is especially useful in small devices and typically preferred to pressure-driven flow owing to its low cost and high efficiency as well as its ability to reduce particle or solute dispersion. A number of recently developed technological applications utilize electrokinetic phenomena as a way to either transport fluid or particles or macromolecules, such as the separation of DNA oligonucleotides by electrophoresis in straight nanochannels [9].

While these phenomena are used ubiquitously in many micro- and nanofluidic devices, their precise modeling is highly complex owing the nontrivial coupling between electrical, chemical and mechanical effects, and is typically limited to relatively simple settings in which simplifying assumptions such as weak field, thin Debye layer, etc. apply. For more complex problems in which these assumptions break down, detailed or accurate models are often still lacking. This is especially true at the nanoscale, where non-continuum effects sometimes become significant, and as the characteristic thickness of the electrical double layers becomes of the same order as the geometric length scales of the device. Previous approaches to tackle this have included continuum models based on the Poisson-Nernst-Planck equations [16], and atomic simulations using molecular dynamics algorithms [17]. While both approaches have their merits, neither of them is easy to use or performs particularly well in applications requiring the modeling of electrokinetic transport in strong confinement and over long time scales.

1.1 Overview

This thesis details the development of a model based on a Langevin equation for diffuse charge dynamics in nanofluidic devices, which incorporates features from both continuum and atomistic methods. The approach, which is presented in detail in chapter 2, can be applied to model both electroosmotic flows in nanochannels and through nanopores, as well as electrophoretic transport of particles or macromolecules. Chapter 3 shows the results of applying the Langevin equation to simulate the model problem of double layer charging in a symmetric binary electrolyte between blocking electrodes that

apply a voltage. Chapter 4 summarizes the results of chapter 3 and draws conclusions based on these findings. The rest of this chapter provides some background on electrokinetic phenomena at small scales and the methods used to model them.

1.2 Background

The phenomenon of electroosmosis has been known for a long time and is illustrated in figure 1.1. [16, 18, 19].

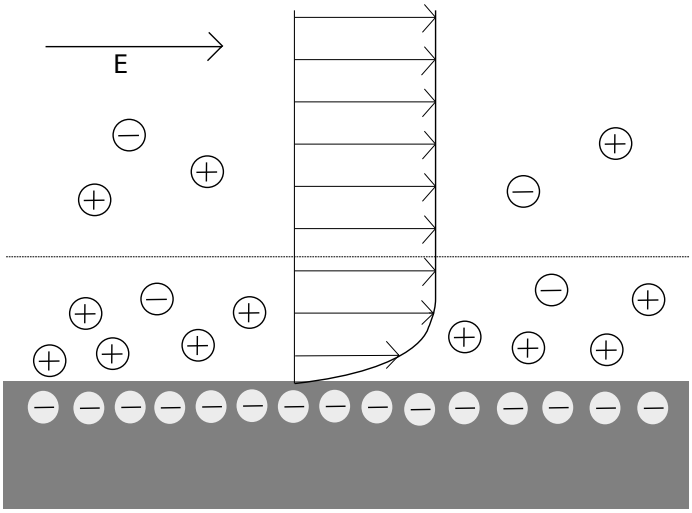

Figure 1.1: Electroosmotic flow near a charged surface

In a micro- or nanochannel, channel walls typically possess a native charge, which attracts ions of opposite sign (*counterions*) in the neighboring electrolyte. These ions accumulate near the charged surface, resulting in the formation of a diffuse charge cloud, also knnown as a Debye layer or electrical double layer (EDL). When an electric field $\boldsymbol{E}_0$ is applied, the net excess charge in the EDL is subject to an electric force which drives the motion of the fluid relative to the fixed surface. In a channel, this phenomenon results in a so-called electroosmotic (EO) flow. The characteristic thickness λ_D of the Debye layer, which is determined by the balance between ion attraction by the charged surface and ion diffusion, is typically of the order of $10 - 100$ μm in aqueous solutions. When this thickness is much less than the channel width (as is typically in the case of microchannels), the effect of the electric

force inside the EDL on the flow outside the EDL is well captured by an effective slip velocity $\boldsymbol{u}_s$, given by the Helmholtz-Smoluchowski equation [20]: $\boldsymbol{u}_s = (\varepsilon_0 \zeta/\mu)\boldsymbol{E}_0$, where ε_0 and μ are the permittivity and viscosity of the fluid, and ζ is the zeta-potential or potential drop across the EDL, and is considered a material constant. This slip velocity can then be shown to drive a potential flow outside of the EDL, which is a plug flow in a unidirectional microchannel [16].

When the Debye thickness λ_D is of the same order as the characteristic geometric scale of the device, as is the case typically in nanochannels, the Helmholtz-Smoluchowski equation is no longer valid and the exact ionic distribution in the channel must be determined in order to evaluate the corresponding force distribution acting on the fluid [21–23] . The classical approach for obtaining this distribution is by solution of the Nernst-Planck equations, which model the ionic conservation (under the effects of diffusion, convection and electromigration), and of the Poisson equation for the determination of the elctric potential in the solution. Knowledge of the excess charge distribution then allows one to obtain the resulting flow velocity field from the Stokes equations including an electric body force. While models based on Poisson-Nernst-Planck (PNP) equations manage to capture qualitative trends in nanochannels, they often fail at providing quantitative results that agree with experiments [21–23]. This is especially true in highly confined environments in which EDLs from opposite walls overlap. Several reasons can be invoked for the breakdown of these models. Specifically, the PNP equations are not able to capture discrete effects, which become more important at very small scales. For instance, steric effects due to the finite size of ions in electrolytes can become significant inside double layers as has been shown in previous studies [24–26], and are not typically accounted for in continuum models, which can often predict ionic concentrations well beyond the close packing limit.

One approach to capture the precise structure of the double layers is obviously molecular dynamics (MD) simulations [17], in which the exact motions of solvent molecules and salt ions are solved for using Newton's equations of motion. MD simulations have been applied successfully to simulate electrokinetic flow in nano-channels, e.g. [27–31]. The advantage of this approach is that it provides detailed information on the structure of the double layers inside the channels down to molecular length scales, and naturally accounts for

noncontinuum effects such as steric effects, structuring of the fluid near the walls, etc. Such simulations, however, are extremely costly owing to the very large number of degrees of freedom and to the very short time scales that need to be resolved. As a result, only very thin and short channels with simple geometries have been simulated, over time scales that are typically much shorter than the relevant dynamic time scales in problems involving particles or macromolecules. The next chapter describes a new approach to model electrokinetic flows in highly confined environments based on a Langevin description of the excess charge dynamics, that incorporates features from both the PNP and MD models.

CHAPTER 2

THEORY

This chapter briefly outlines the continuum dilute solution theory that is traditionally used to describe the electro-diffusion of ions and electrokinetic phenomena. The Langevin approach is detailed in section 2.3, and the setup for the model problem simulated in this study is described in section 2.4. It is assumed for simplicity that we are dealing with a symmetric binary (*z:z*) electrolyte.

2.1 The Poisson-Boltzmann equation

The standard model of electro-diffusion is based on the assumption that the ions of a species i in a dilute solution are in quasi-thermal equilibrium with a Boltzmann distribution [32, 33]:

$$c_i = c_i^0 e^{-z_i e\phi/kT} \tag{2.1}$$

where c_i^0 is a reference concentration, z is the valence, e is the elementary charge, and kT is the thermal energy of the liquid. The electrostatic potential ϕ is given (in a mean-field approximation) by Poisson's equation:

$$\varepsilon_0 \nabla^2 \phi = -\sum_i z_i e c_i \tag{2.2}$$

Together, we get the Poisson-Boltzmann equation,

$$\nabla^2 \phi = -\sum_i z_i e c_i^0 e^{-z_i e\phi/kT}. \tag{2.3}$$

Equation 2.3 must be solved numerically except when linearized under the assumption that the potential is much lower than the thermal voltage ($|\phi| \ll$

$kT/z_i e$). In the linearized limit, for a symmetric binary (z:z) electrolyte in a one-dimensional geometry, the Poisson-Boltzmann (PB) equation was solved analytically by Gouy and Chapman for a semi-infinite electrolyte near a charged surface [32, 33]. (This describes the most common conditions under which an electrical double layer forms.) The PB equation reduces to $\varepsilon_0 \frac{\partial^2 \phi}{\partial x^2} = 2zec_0 \sinh(\frac{ze\phi}{kT})$. The characteristic width of the diffuse double layer, obtained by nondimensionalizing the PB equation,

$$\lambda_D = \sqrt{\frac{\varepsilon_0 kT}{2z^2 e^2 c_0}} \tag{2.4}$$

is called the Debye screening length.

2.2 The Poisson-Nernst-Planck equations

When the assumption of quasi-thermal equilibrium cannot be made, such as in electrolytes subject to time-dependent applied voltages, the Boltzmann distribution no longer holds, and the description must now include a conservation equation for each species of ion.

The classical description comes from the Poisson-Nernst-Planck equations, which consist of Poisson's equation (2.2) and mass conservation laws for the ions:

$$\frac{\partial c_i}{\partial t} + \boldsymbol{\nabla} \cdot (-\mu_i c_i z e \boldsymbol{\nabla} \phi - \mu_i c_i kT \boldsymbol{\nabla} \log c_i + \boldsymbol{u}) = 0 \tag{2.5}$$

where μ_i is the mobility of species i and $\boldsymbol{u}$ is the local fluid velocity. This equation holds as long as the flux of species i remains proportional to the gradient of its chemical potential, *i.e.*, while

$$\boldsymbol{v}_i = -D_i(\boldsymbol{\nabla} c_i + \frac{z_i e}{kT} c_i \boldsymbol{\nabla} \phi) \tag{2.6}$$

where $\boldsymbol{v}_i$ is the flux of species i. D_i is the diffusivity, related to the mobility through Einstein's relation [32], $\mu_i = D_i kT$.

These continuum models are often used to model the diffuse layer at large applied potentials, but have limited applicability due to the exponential sensitivity of counterion concentration to voltage. For instance, there exists a maximum possible concentration of ions near a surface in the "close packing"

limit, and the Poisson-Boltzmann equation overpredicts the concentration at applied voltages that are just a few times the thermal voltage (kT/z_ie).

2.3 The Langevin approach

As discussed in chapter 1, existing models for electroosmotic flow in highly confined devices suffer from several limitations. Continuum models based on the PNP equations are highly complex and difficult to solve even numerically, and fail to capture a number of phenomena which result from the discrete nature of the electrical double layers. Atomistic models based on MD simulations provide excellent resolution but are extremely costly and only allow the simulations of very small devices with simple geometries over short time scales.

The basis for the proposed methodology is the observation that the solution of the Nernst-Planck equations is strictly equivalent to an ensemble average over a collection of charged Brownian particles (representing the ionic species in the EDL) undergoing a stochastic motion satisfying an appropriate Langevin stochastic differential equation. Specifically, the Nernst-Planck equation (2.5) rewritten for the positively and negatively charged ion densities $c_\pm$ is:

$$\frac{\partial c_\pm}{\partial t} + \boldsymbol{\nabla} \cdot (c_\pm \boldsymbol{v}_\pm) = 0 \tag{2.7}$$

where the flux velocities $\boldsymbol{v}_\pm$ are given by:

$$\boldsymbol{v}_\pm = \mp \mu z e \boldsymbol{\nabla}\phi - kT\mu \boldsymbol{\nabla} \log c_\pm + \boldsymbol{u}, \tag{2.8}$$

where μ is the mobility of an ion in the solvent and $\boldsymbol{u}$ is the local fluid velocity. The electric potential ϕ is obtained by solving Poisson's equation (2.2) modified for a symmetric binary electrolyte:

$$\nabla^2 \phi = -\frac{(c_+ - c_-)ze}{\varepsilon_0} \tag{2.9}$$

Because equation (2.7) is simply an advection-diffusion equation, its solution is equivalent to an ensemble average over trajectories of Brownian particles obeying the following Langevin equation, for instance for a positively charged

ion of index n with position $\boldsymbol{x}_n^+$:

$$\mathrm{d}\boldsymbol{x}_n^+ = (-\mu z e \boldsymbol{\nabla}\phi + \boldsymbol{u})dt + \sqrt{\frac{2kTdt}{\mu}}\boldsymbol{n} \tag{2.10}$$

where $\boldsymbol{n}$ is a random Gaussian variable with zero mean and unit variance. The electric potential now satisfies a discrete version of Poisson's equation:

$$\nabla^2\phi = -\frac{ze}{\varepsilon_0}\sum_n \pm\delta(\boldsymbol{x} - \boldsymbol{x}_n^{\pm}) \tag{2.11}$$

where the sum is now over all the ions in the solution and δ denotes the Dirac delta function.

This formulation can be used to simulate double layer formation as follows. First, the charge distribution in the electrolytes is determined by Brownian dynamics simulations. Electric interactions between ions are modeled either directly as Coloumb interactions between point charges, or from a mean-field description of the induced field obtained by extrapolating the excess charges to a grid. The Langevin equation is then used to advance the charges.

2.4 The model problem

The simulation carried out in this study is of double layer charging in a symmetric *z:z* binary electrolyte between parallel plate blocking electrodes that suddenly apply a voltage at $t = 0$. The local fluid velocity $\boldsymbol{u}$ is assumed to be zero everywhere. This model problem helps provide easy comparisons between the different approaches discussed above.

Two parallel blocking electrode plates are maintained a distance L apart, where L is much smaller than the extent of the electrodes along their other dimensions. The space in between is filled with a symmetric binary $z : z$ electrolyte that has no excess charge to begin with. At $t = 0$, a voltage V is applied across the elctrodes, causing the formation of electrical double layers near both electrodes.

We use as our domain a cube of side L, enforcing periodic boundary conditions on all "open" sides. Considering N ions (particles) of either polarity in the domain, the Langevin equation from the previous section that applies to each of them is

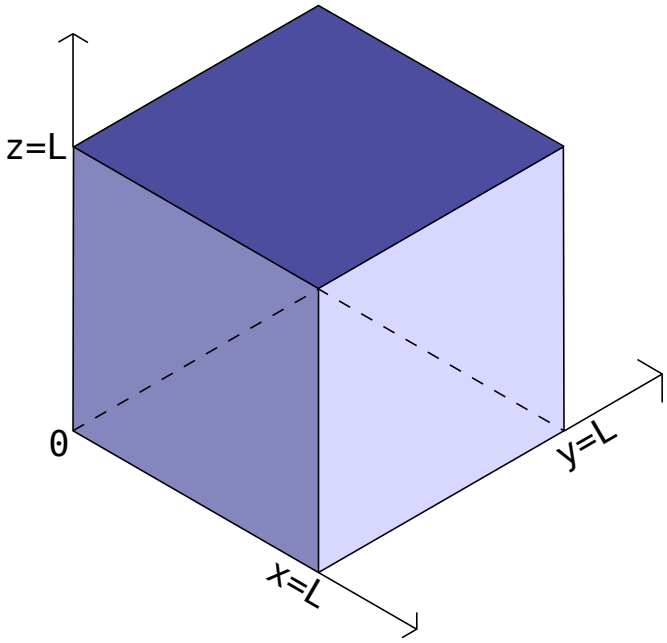

Figure 2.1: The domain of simulation in section 2.4

$$\mathrm{d}\boldsymbol{x}_i^+ = -\mu z e \boldsymbol{\nabla}\phi dt + \sqrt{\frac{2kTdt}{\mu}}\boldsymbol{n} \tag{2.12}$$

At each time step, each particle is advanced in accordance with equation 2.12. The potential then needs to be solved for using a suitable Poisson's equation.

Two approaches to finding the potential are considered here:

- It can be found in terms of the mean field induced by extrapolating the charges to a grid and using the discrete Fourier transform to solve for the potential on the grid, or
- It can be solved for by modeling the ions as point charges together with an efficient particle-mesh algorithm, in this case, a smooth particle-mesh Ewald (SPME) algorithm.

In the first case, the relevant Poisson's equation is simply $\varepsilon_0 \nabla^2 \phi = -\rho$, where ρ is the interpolated charge density. In the second case, the relevant Poisson's equation is given by equation 2.11.

Once the potential has been found, the particle positions are updated again.

When suitably nondimensionalized, there is only one parameter, the ratio of the Debye screening length (equation 2.4) to the length scale of interest, in addition to the applied voltage. The scaling involved and nondimensional forms of the governing equations may be found in appendix A.2.

2.5 Solving Poisson's equation

2.5.1 Mean field solution using the discrete Fourier transform

This section describes the solution of Poisson's equation:

$$\varepsilon_0 \nabla^2 \phi = -\rho \tag{2.13}$$

over the unit cube $0 \leq x < 1$, $0 \leq y < 1$, $0 \leq z \leq 1$, with periodic boundary conditions in the x and y directions, and Dirichlet boundary conditions at $z = 0$ and $z = 1$, $\phi(z = 0) = v_1, \phi(z = 1) = v_2$.

In general, the solution may be sought as the superposition of two potentials ϕ_h and ϕ. ϕ_h satisfies Laplace's equation on the unit cube, is periodic in x and y with period 1, and satisfies the given boundary conditions on $z = 0, 1$. ϕ satisfies Poisson's equation on the unit cube, periodic boundary conditions along $x = 0, 1$, $y = 0, 1$, and vanishes at $z = 0, 1$. ϕ_h is easily solved for analytically, while ϕ is solved for below.

Since the potential ϕ is periodic along x and y, we can write ϕ as a superposition of Fourier modes along these directions. Further, since the potential vanishes at the bottom and top walls, we can write ϕ as a superposition of sines of various wavelengths along z. That is,

$$\phi(x, y, z) = \sum_{k=1}^{\infty} \sum_{i=-\infty}^{\infty} \sum_{j=-\infty}^{\infty} \Phi_{ijk} e^{2\pi I(ix+jy)} \sin(\pi k z) \tag{2.14}$$

where $I^2 = -1$. The density ρ can be similarly decomposed into its Fourier modes:

$$\rho(x, y, z) = \sum_{k=1}^{\infty} \sum_{i=-\infty}^{\infty} \sum_{j=-\infty}^{\infty} R_{ijk} e^{2\pi I(ix+jy)} \sin(\pi k z) \tag{2.15}$$

Substituting these expressions into Poisson's equation we get, after some

algebra,

$$\varepsilon_0 \sum_{k=1}^{\infty} \sum_{i=-\infty}^{\infty} \sum_{j=-\infty}^{\infty} \left(-4\pi^2 i^2 - 4\pi^2 j^2 - \pi^2 k^2\right) \Phi_{ijk} e^{2\pi I(ix+jy)} \sin(\pi k z) = \\ -\sum_{k=1}^{\infty} \sum_{i=-\infty}^{\infty} \sum_{j=-\infty}^{\infty} R_{ijk} e^{2\pi I(ix+jy)} \sin(\pi k z) \quad (2.16)$$

Invoking the property of orthonormality of the complex exponentials and the sines, we can find the amplitude of any mode of ϕ (corresponding to a given i, j, k) as:

$$\Phi_{ijk} = \frac{R_{ijk}}{\varepsilon_0 \pi^2 \left(4i^2 + 4j^2 + k^2\right)} \quad (2.17)$$

And the solution ϕ can be reconstructed in accordance with equation 2.14.

In practice, with $\rho(x, y, z)$ known only at a finite number of grid points in the domain, the discrete Fourier and Sine transforms need to be used, which provide only a finite number of modes equal to the number of grid points. Nevertheless, the use of Fast Fourier Transform algorithms (FFTs) makes solving for the potential an efficient and fast process.

2.5.2 Solution using SPME

This section derives the solution of Poisson's equation:

$$\varepsilon_0 \nabla^2 \phi = -\sum_n q_n \delta(\boldsymbol{r} - \boldsymbol{r}_n) \quad (2.18)$$

with a periodic distribution of N point charges using a Smooth Mesh Particle Ewald (SPME) method [34,35]. The domain is a cell of volume $\tau_0 = L^3$, with the same boundary conditions that apply to the model problem: periodic boundary conditions along x and y (with period L), and $\phi(z = 0) = v_1, \phi(z = L) = v_2$.

The potential Φ is treated as the superimposition of three potentials, $\Phi = \phi_h + \phi + \phi_b$, where

1. ϕ_h satisfies Laplace's equation with periodic boundary conditions along the x, y faces of the cell and with $\phi_h(z = 0) = v_1$, $\phi_h(z = L) = v_2$,

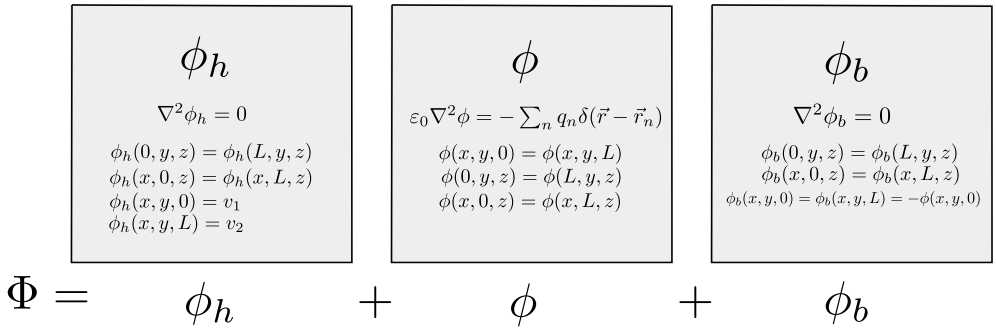

Figure 2.2: Breakup of Φ for solution using SPME, section 2.5.2

2. ϕ satisfies Poisson's equation (2.18) with periodic boundary conditions at all boundaries, and

3. ϕ_b satisfies Laplace's equation that satisfies periodic boundary conditions along the x, y faces of the cell, and satisfies $\phi_b(z = 0) = \phi_b(z = L) = -\phi(z = 0) = -\phi(z = L)$. (The last equality holds automatically from the boundary conditions on ϕ.)

The sum of the three potentials Φ then satisfies equation (2.11) with the correct boundary conditions (figure 2.2).

ϕ_h can be solved for analytically, since v_1 and v_2 are constants. ϕ is solved for using the Smooth Mesh Particle Ewald method described below, and ϕ_b is solved using the discrete Fourier transform.

Finding ϕ using SPME

The expression $\sum_n q_n\delta(\boldsymbol{r} - \boldsymbol{r}_n)$ has a Fourier series expansion given by:

$$\frac{1}{\tau_0}\sum_{\boldsymbol{k}}\sum_n q_n e^{-2\pi I(\boldsymbol{k}\cdot(\boldsymbol{r}-\boldsymbol{r}_n))}$$

where $\boldsymbol{k}$ is the tuplet of wavenumbers (k_1, k_2, k_3) and the term $\sum_{\boldsymbol{k}}$ is assumed to mean the triple sum $\sum_{k_1}\sum_{k_2}\sum_{k_3}$.

Assuming the Fourier series expansion $\sum_{\boldsymbol{k}}\phi_{\boldsymbol{k}}e^{-2\pi I\boldsymbol{k}\cdot\boldsymbol{r}}$ for the potential ϕ and substituting these forms for the potential and the density into Poisson's equation, we get

$$\varepsilon_0 \nabla^2 \left[\sum_{\boldsymbol{k}} \phi_{\boldsymbol{k}} e^{-2\pi I \boldsymbol{k}\cdot\boldsymbol{r}} \right] = -\sum_{\boldsymbol{k}} \sum_{n} (q_n/\tau_0) e^{-2\pi I(\boldsymbol{k}\cdot(\boldsymbol{r}-\boldsymbol{r}_n))}$$
$$4\pi^2 \varepsilon_0 \sum_{\boldsymbol{k}} k^2 \phi_k e^{-2\pi I \boldsymbol{k}\cdot\boldsymbol{r}} = \sum_{\boldsymbol{k}} \sum_{n} (q_n/\tau_0) e^{-2\pi I(\boldsymbol{k}\cdot(\boldsymbol{r}-\boldsymbol{r}_n))}$$

where $k^2 = \boldsymbol{k}\cdot\boldsymbol{k}$. Invoking the orthogonality of modes corresponding to distinct wavenumbers, we get

$$\phi_{\boldsymbol{k}} = \frac{1}{4\pi^2 \varepsilon_0 \tau_0} \sum_n \frac{q_n e^{2\pi I \boldsymbol{k}.\boldsymbol{r_n}}}{k^2}, \qquad \boldsymbol{k} \neq \boldsymbol{0}$$
$$\phi(\boldsymbol{r}) = \frac{1}{4\pi^2 \varepsilon_0 \tau_0} \sum_n \left(q_n \sum_{\boldsymbol{k}\neq\boldsymbol{0}} \frac{e^{-2\pi I \boldsymbol{k}\cdot(\boldsymbol{r}-\boldsymbol{r}_n)}}{k^2} \right) \tag{2.19}$$

The case of $\boldsymbol{k} = \boldsymbol{0}$ simply gives $\sum_n q_n = 0$, implying charge neutrality. (In the absence of charge neutrality, Poisson's equation with a periodic distribution of point charges does not have a finite solution.)

Now consider

$$\frac{1}{k^{2m}} = \frac{\pi^m}{\Gamma(m)} \int_0^\infty e^{-\pi k^2 \beta} \beta^{m-1} \mathrm{d}\beta$$
$$\sigma_{mn} = \sum_{\boldsymbol{k}\neq\boldsymbol{0}} \frac{e^{-2\pi I \boldsymbol{k}\cdot(\boldsymbol{r}-\boldsymbol{r}_n)}}{k^{2m}} = \frac{\pi^m}{\Gamma(m)} \sum_{\boldsymbol{k}\neq\boldsymbol{0}} \int_0^\infty e^{-\pi k^2 \beta - 2\pi I \boldsymbol{k}\cdot(\boldsymbol{r}-\boldsymbol{r}_n)}$$

so that the potential ϕ is simply

$$\phi(\boldsymbol{r}) = \frac{1}{4\pi^2 \varepsilon_0 \tau_0} \sum_n q_n \sigma_{1n}$$
$$= \frac{1}{4\pi^2 \varepsilon_0 \tau_0} \sum_n q_n \frac{\pi}{\Gamma(1)} \sum_{\boldsymbol{k}\neq\boldsymbol{0}} \int_0^\infty e^{-\pi k^2 \beta - 2\pi I \boldsymbol{k}\cdot(\boldsymbol{r}-\boldsymbol{r}_n)} \mathrm{d}\beta \tag{2.20}$$

We now introduce a parameter α, the Ewald coefficient, by way of splitting the integral above:

$$\int_0^\infty e^{-\pi k^2\beta - 2\pi I \boldsymbol{k}\cdot(\boldsymbol{r}-\boldsymbol{r_n})}\mathrm{d}\beta = \int_0^\alpha e^{-\pi k^2\beta - 2\pi I \boldsymbol{k}\cdot(\boldsymbol{r}-\boldsymbol{r_n})}\mathrm{d}\beta + \int_\alpha^\infty e^{-\pi k^2\beta - 2\pi I \boldsymbol{k}\cdot(\boldsymbol{r}-\boldsymbol{r_n})}\mathrm{d}\beta$$

Next, we apply Ewald's θ-transformation formula (derived by applying Poisson's summation formula to the Gaussian $e^{-\pi(\boldsymbol{r}-\boldsymbol{r}_n)^2/\beta}$):

$$\sum_{\boldsymbol{k}\neq\boldsymbol{0}} e^{-\pi k^2\beta - 2\pi I \boldsymbol{k}\cdot\boldsymbol{r}} = \frac{\tau_0}{\beta^{3/2}} \sum_l e^{-\frac{\pi(\boldsymbol{r}-\boldsymbol{r}_l)^2}{\beta}} \tag{2.21}$$

to the integral from 0 to α. We get:

$$\sum_{\boldsymbol{k}\neq\boldsymbol{0}} \int_0^\infty e^{-\pi k^2\beta - 2\pi I \boldsymbol{k}\cdot(\boldsymbol{r}-\boldsymbol{r}_n)}\mathrm{d}\beta = \int_0^\infty \left(\frac{\tau_0}{\beta^{3/2}} \sum_l e^{-\pi(\boldsymbol{r}-\boldsymbol{r}_n-\boldsymbol{r}_l)^2/\beta} - 1 \right) \mathrm{d}\beta + \sum_{\boldsymbol{k}\neq\boldsymbol{0}} \int_\alpha^\infty e^{-\pi k^2\beta - 2\pi I \boldsymbol{k}\cdot(\boldsymbol{r}-\boldsymbol{r}_n)}\mathrm{d}\beta \tag{2.22}$$

Effectively, the infinite sum over $\boldsymbol{k}$ is split into two sums, one carried out in real space and the other in Fourier space as before.

Defining the incomplete Gamma function $\psi_n(x) = \int_1^\infty t^n e^{-xt}\mathrm{d}t$, and writing the above integrals in equation (2.22) in terms of $\psi_{-1/2}$ and ψ_0 respectively, we get

$$\begin{aligned}\sigma_{1n} =& \frac{\pi\alpha}{\Gamma(1)} \left[\tau_0 \alpha^{-3/2} \sum_l \psi_{-1/2}\left(\frac{\pi(\boldsymbol{r}-\boldsymbol{r}_n-\boldsymbol{r}_l)^2}{\alpha} \right) \right] \\ &+ \frac{\pi\alpha}{\Gamma(1)} \left[\sum_{\boldsymbol{k}\neq\boldsymbol{0}} e^{-2\pi I \boldsymbol{k}\cdot(\boldsymbol{r}-\boldsymbol{r}_n)} \psi_0(\pi\alpha k^2) - 1 \right]\end{aligned} \tag{2.23}$$

Substituting this expression in equation 2.20, we get an expression for the

potential ϕ:

$$\begin{aligned}\phi(\boldsymbol{r}) =& \frac{\pi\alpha}{4\pi^2\varepsilon_0\tau_0}\left[\tau_0\alpha^{-3/2}\sum_n\sum_l q_n\psi_{-1/2}\left(\frac{\pi(\boldsymbol{r}-\boldsymbol{r}_n-\boldsymbol{r}_l)^2}{\alpha}\right)\right] \\ &+\frac{\pi\alpha}{4\pi^2\varepsilon_0\tau_0}\left[\sum_{\boldsymbol{k}\neq\boldsymbol{0}}\left(\sum_n q_n e^{-2\pi I\boldsymbol{k}\cdot(\boldsymbol{r}-\boldsymbol{r}_n)}\right)\psi_0(\pi\alpha k^2)-\sum_n q_n\right].\end{aligned}$$

The term $\sum_n q_n$ is zero due to charge neutrality, so

$$\begin{aligned}\phi(\boldsymbol{r}) =& \frac{\alpha}{4\pi\varepsilon_0\tau_0}\left[\tau_0\alpha^{-3/2}\sum_n\sum_l q_n\psi_{-1/2}\left(\frac{\pi(\boldsymbol{r}-\boldsymbol{r}_n-\boldsymbol{r}_l)^2}{\alpha}\right)\right] \\ &+\frac{\alpha}{4\pi\varepsilon_0\tau_0}\left[\sum_{\boldsymbol{k}\neq\boldsymbol{0}}\left(\sum_n q_n e^{-2\pi I\boldsymbol{k}\cdot(\boldsymbol{r}-\boldsymbol{r}_n)}\right)\psi_0(\pi\alpha k^2)\right].\end{aligned} \tag{2.24}$$

The field acting on the charges is $-\nabla\phi(\boldsymbol{r})$, which can be calculated from equation (2.24) and used directly in the Langevin equation (2.12). After some algebra, we get

$$\begin{aligned}-\nabla\phi(\boldsymbol{r}) =& \boldsymbol{E}(\boldsymbol{r}) = \sum_l\sum_n \boldsymbol{A}(\alpha,\boldsymbol{r}-\boldsymbol{r}_n-\boldsymbol{r}_l)q_n \\ &+\sum_{\boldsymbol{k}\neq\boldsymbol{0}} e^{-2\pi I\boldsymbol{k}\cdot\boldsymbol{r}}\boldsymbol{B}(\alpha,\boldsymbol{k})\left(\sum_n q_n e^{2\pi I\boldsymbol{k}\cdot\boldsymbol{r_n}}\right)\end{aligned} \tag{2.25}$$

where $\boldsymbol{A}$ and $\boldsymbol{B}$ are given by:

$$\begin{aligned}\boldsymbol{A}(\alpha,\boldsymbol{r}) &= \frac{1}{2\varepsilon_0\alpha^{3/2}}\psi_{1/2}\left(\frac{\pi(\boldsymbol{r}\cdot\boldsymbol{r})}{\alpha}\right)\boldsymbol{r} \\ \boldsymbol{B}(\alpha,\boldsymbol{k}) &= \frac{I\alpha}{2\varepsilon_0\tau_0}\psi_0(\pi\alpha k^2)\boldsymbol{k}\end{aligned}$$

Finding ϕ_b using the DFT

We intend to solve $\nabla^2\phi_b = 0$ with periodic boundary conditions along the x and y faces, and with $\phi_b(z=0) = \phi_b(z=L) = -\phi(z=0)$.

Since ϕ_b is periodic along x and y, we can assume a Fourier series of the

form:

$$\phi_b(\boldsymbol{r}) = \sum_{\boldsymbol{k}} \phi_{b,\boldsymbol{k}}(z) e^{-2\pi I \boldsymbol{k}\cdot\boldsymbol{R}} \tag{2.26}$$

where vck is the 2-tuple (k_x, k_y) and $\boldsymbol{R}$ equals (x, y).

Substituting this form into Laplace's equation and invoking the orthogonality of modes corresponding to distinct wavenumbers yields an ordinary differential equation:

$$\frac{d^2\phi_{b,\boldsymbol{k}}}{dz^2} = k^2 \phi_{b,\boldsymbol{k}}(z) \tag{2.27}$$

where $k^2 = k_x^2 + k_y^2$. This ODE has the solution:

$$\phi_{b,\boldsymbol{k}} = A_{\boldsymbol{k}} e^{kz} + B_{\boldsymbol{k}} e^{-kz} \tag{2.28}$$

The boundary conditions at $z = 0$ and $z = L$ can now be applied. Since $\phi(z = 0)$ is known, its Fourier series expansion can be determined:

$$\phi(z = 0) = \sum_{\boldsymbol{k}} \phi_{0,\boldsymbol{k}} e^{-2\pi I \boldsymbol{k}\cdot\boldsymbol{R}}$$

And invoking the orthogonality of distinct modes again, we get:

$$\begin{aligned} A_{\boldsymbol{k}} + B_{\boldsymbol{k}} &= \phi_{0,\boldsymbol{k}} \\ A_{\boldsymbol{k}} e^{kL} + B_{\boldsymbol{k}} e^{-kL} &= \phi_{0,\boldsymbol{k}} \end{aligned}$$

So that $A_{\boldsymbol{k}} = \frac{(1-e^{-kL})\phi_{0,\boldsymbol{k}}}{e^{kL}-e^{-kL}}$, $B_{\boldsymbol{k}} = \frac{(e^{kL}-1)\phi_{0,\boldsymbol{k}}}{e^{kL}-e^{-kL}}$, and $\phi_b(\boldsymbol{r})$ is given by:

$$\phi_b(\boldsymbol{r}) = \sum_{\boldsymbol{k}} \phi_{0,\boldsymbol{k}} \frac{e^{kz}(1-e^{-kL}) + e^{-kz}(e^{kL}-1)}{e^{kL}-e^{-kL}} \tag{2.29}$$

Which is used to find the actual potential along with $\phi(\boldsymbol{r})$ determined from the SPME method above. In practice, the Fourier series expansion of $\phi(z = 0)$ is found in terms of a two-dimensional discrete Fourier transform.

2.6 Handling steric interactions

The assumption that the ions are point charges is a poor one at sufficiently high concentrations. Such high concentrations are reached near the electrodes

(or charged surfaces) even in otherwise dilute solutions at voltages that are only a few times higher than the thermal voltage. In reality, there is a steric limit to the concentration of ions that can be achieved in any double layer.

To model these steric effects, we consider our ions to be spherical particles of effective size (radius) a that cannot overlap. In physical situations, a is clearly no less than the ionic radius, of the order of 1Å.

Particles of finite size undergo collisions which need to be accounted for. A contact algorithm that prevents overlaps is therefore used [36], the details of which are as follows. At each time step t_i, let $\delta \boldsymbol{x}_n^i$ be the displacement of particle n over the next time step if potential overlaps are ignored. The set of particles m ($m = 1, 2, .., M$) that overlap with particle n in this time step can be determined by checking whether $|\boldsymbol{x}_n^{i+1} - \boldsymbol{x}_m^{i+1}| < 2a$. For each particle m that overlaps with n, the fraction of Δt after which surface contact occurs can be determined, assuming the particles move at constant speeds during this time step. The fraction Δt_c^{mn} is given by the equation:

$$|\boldsymbol{x}_n^i - \boldsymbol{x}_m^i + (\delta \boldsymbol{x}_n^i - \delta \boldsymbol{x}_m^i)\Delta t_c^{mn}/\Delta t|^2 = 4a^2$$

Only the root that lies in the interval $[0, \Delta t]$ is chosen. The particles $m = 1, ..., M$ are sorted in increasing order of Δt_c^{mn}, so that $\Delta t_c^{1n} \leq ... \leq \Delta t_c^{Mn}$. Finally, the particle n is moved back to its original position $\boldsymbol{x}_n^i$, and for each particle $m = 1, ..., M$, moved a fraction $\Delta t_c^{mn}/\Delta t$ of the full time step in the direction in which overlap would otherwise occur with particle m. In the normal directions, it is moved a full time step. This is summarized in the following expression, which can be verified to prevent all overlaps:

$$\begin{aligned} \boldsymbol{x}_n^{i+1} = \boldsymbol{x}_n^i + \sum_{m=1}^{M} \widehat{\boldsymbol{R}_{mn}^i}\widehat{\boldsymbol{R}_{mn}^i} \cdot \left[\prod_{k=1}^{M-1} \left(\boldsymbol{I} - \widehat{\boldsymbol{R}_{mk}^i}\widehat{\boldsymbol{R}_{mk}^i}\right)\right] \cdot \delta \boldsymbol{x}_{\boldsymbol{n}}^{\boldsymbol{i}} \\ + \left[\prod_{m=1}^{M} \left(\boldsymbol{I} - \widehat{\boldsymbol{R}_{mn}^i}\widehat{\boldsymbol{R}_{mn}^i}\right)\right] \cdot \delta \boldsymbol{x}_n^i \end{aligned} \tag{2.30}$$

where $\widehat{\boldsymbol{R}_{mn}^i}$ is the unit vector pointing from sphere n to sphere m. When $m = 1$, the product over k is replaced by the identity tensor.

Since the position of each particle needs to be checked against the position of all the other particles at each time step, this is a computationally expensive

endeavor ($O(N^2)$). The interaction between particles is very close range (indeed, only at contact), so a cell list may be employed to significantly speed up the bookkeeping involved [17]. The domain is divided into cells and a frequently updated list of the contents of each cell is maintained. At each time step, only the members of neighboring cells need to be scanned for overlap, which significantly reduces the number of checks needed.

2.7 Boundary conditions

In general, the electrodes at $z = 0, L$ will possess a thin layer of surface charge that is comprised of ions adsorbed directly onto the surface. This *Stern layer* may be accounted for by modifying the potential at $z = 0, L$ (originally v_1, v_2) [32]:

$$\phi(z = 0) = v_1 + \lambda_s \left(\frac{\partial \phi}{\partial z}\right)_{z=0}$$
$$\phi(z = L) = v_2 - \lambda_s \left(\frac{\partial \phi}{\partial z}\right)_{z=L}$$

where λ_s is an effective thickness for the Stern layer. For a simple dielectric layer, this equals the actual thickness times the ratio ϵ/ϵ_s of dielectric constants of the solvent, ϵ, and the Stern layer, ϵ_s. The Stern layer is always of molecular dimensions, and in most microelectrochemical systems, the ratio of the widths of the Stern layer to the Debye layer is vanishingly small [32]. The presence of the Stern layer thus does not affect the results of the simulation in most cases, and the original boundary conditions discussed in section (2.4) may be used without significant error.

There are multiple ways to enforce zero flux boundary conditions at the walls [37]. The most commonly used method is to carry out specular reflections of particle trajectories at either wall. If $\boldsymbol{x}_n^i$ is the position of particle n at the current timestep i and $\boldsymbol{x}_n^{i+1} = \boldsymbol{x}_n^i + \Delta \boldsymbol{x}_n$ is the new position, where the new z coordinate $z_n^i + \Delta z_n \notin [0, L]$, then

$$\boldsymbol{x}_n^{i+1} = (\boldsymbol{I} - 2\hat{\boldsymbol{n}}\hat{\boldsymbol{n}}) \cdot \left(\boldsymbol{x}_n^i + \Delta \boldsymbol{x_n}\right)$$

where $\hat{\boldsymbol{n}}$ is the unit vector normal to the boundary of interest.

In addition, two other methods that have been proposed are:

- *Rejection*: The particle does not change its position in the current time step, $\Delta \boldsymbol{x}_n = 0$.
- *Multiple Rejection*: New increments are calculated until a $\Delta \boldsymbol{x}_n$ is found such that $z_n^i + \Delta z_n \in [0, L]$.

It is noted that only the specular reflection method correctly imposes the zero flux boundary condition, and all other methods lead to incorrect concentration profiles in the immediate vicinity of the boundary [37].

2.8 Steady state solution of the PNP equations

To compare the results of the simulation driven by the Langevin formulation of the governing equations to the classical PNP equations, it is helpful to consider the one-dimensional version of the PNP equations. In one dimension, these equations are:

$$\frac{\partial c_\pm}{\partial t} = -\frac{\partial}{\partial X}\left(-D\frac{\partial c_\pm}{\partial X} \mp \mu z e c_\pm \frac{\partial \phi}{\partial X}\right) \tag{2.31}$$

$$-\varepsilon_0 \frac{\partial^2 \phi}{\partial X^2} = ze(c_+ - c_-) \tag{2.32}$$

The electrodes at either end are blocking electrodes without Faradaic processes, so the ionic fluxes (equation 2.6) must vanish there. The boundary conditions are thus:

$$-D\frac{\partial c_\pm}{\partial X} \mp \frac{zeD}{kT} c_\pm \frac{\partial \phi}{\partial X} = 0 \qquad X = 0, L \tag{2.33}$$

$$\phi = V \qquad X = 0, \qquad \phi = 0 \qquad X = L \tag{2.34}$$

With a suitable change of variables, these reduce at steady state to a coupled system of nonlinear ordinary differential equations that are easily solved numerically (appendix A.1). The steady state density and potential can then be compared to their values from the three dimensional simulation using the Langevin formulation averaged at $x - y$ cross-sections.

CHAPTER 3

RESULTS AND DISCUSSION

3.1 Model parameters

As explained in section 2.4, there are only two parameters governing the dynamics of the double layer formations. To emphasize the importance of diffuse charge, we choose a value of $\lambda_D/L = 0.025$ that is fairly large. This corresponds to, say, $\lambda_D = 5nm, L = 200nm$, which is fairly characteristic of a micro-electrochemical system.

The other parameter is the (nondimensional) applied voltage ($v = zeV/kT$). We choose $v = 0.1$ and $v = 2$, corresponding to voltages of 2.5 and $25mV$ respectively at room temperature for monovalent ions [38].

3.2 Comparison of results

Representative snapshots of the domain with 300 particles are shown at various time steps in the simulation in figure 3.1.

At steady state, the potential and density are averaged over each $x - y$ cross-section and over several timesteps. Comparisons of the obtained profiles and the numerical solution of the one-dimensional PNP equations are plotted in figures 3.2 and 3.3.

The profiles obtained by the averaged simulation results and by solution of the one-dimensional PNP equations are found to agree.

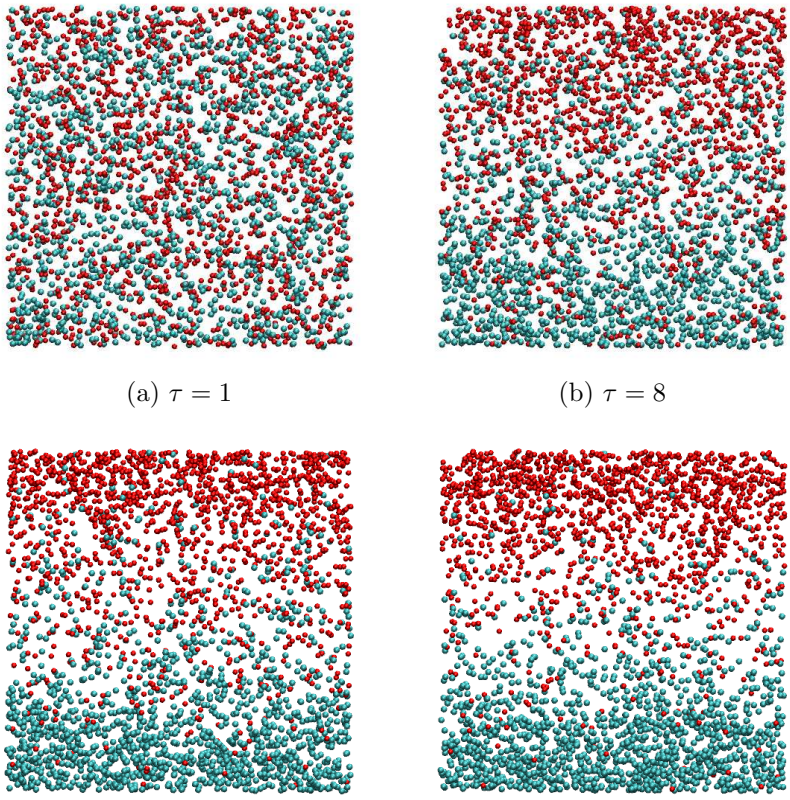

(a) $\tau = 1$ (b) $\tau = 8$

(c) $\tau = 20$ (d) $\tau = 60$

Figure 3.1: Snaps of the domain at various stages of double layer formation.

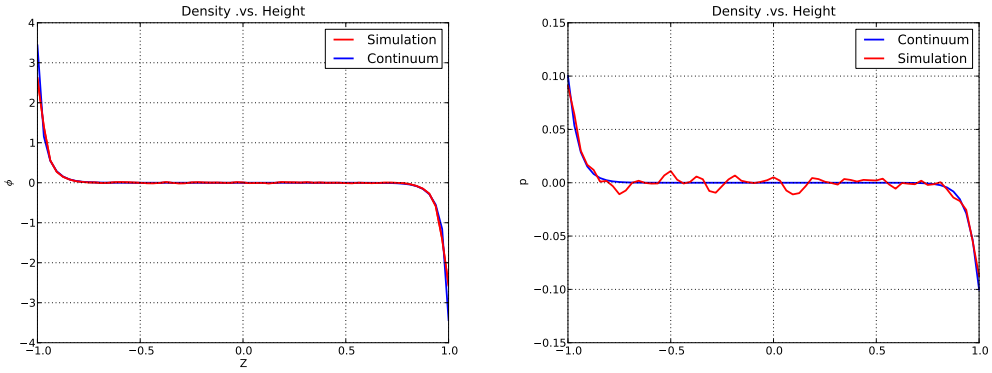

(a) $v = 2.0$ (b) $v = 0.1$

Figure 3.2: Steady state density profile as a function of Z, as predicted by the simulation and the PNP equations.

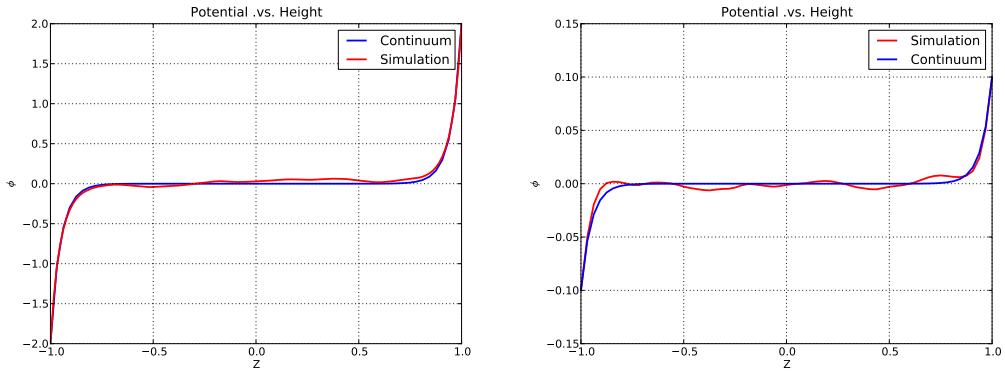

(a) $v = 2.0$ (b) $v = 0.1$

Figure 3.3: Steady state potential as a function of Z, as predicted by the simulation and the PNP equations.

CHAPTER 4

CONCLUSIONS AND FUTURE WORK

The equivalence of the PNP equations and the Langevin formulation developed in chapter 2 has been tested for the case of double layer charging in a symmetric binary electrolyte between parallel plate blocking electrodes. It is observed that there are slight discrepancies in the predicted density at the walls for the voltages considered. This can be attributed to the limited resolution afforded by the grid to which the electric charge and field are interpolated.

As discussed in chapter 2, an efficient way of calculating the electric interaction between (effectively) point charges is to use the SPME algorithm, which is based on a decomposition of the periodic Green's functions for Laplace's equation. A natural extension of this approach is to apply the SPME algorithm to the solution of Stokes equations as well, which will couple the motion of the charges in the electric field to the flow of the electrolyte.

The SPME algorithm also implicitly assumes a periodic geometry and does not directly account for interactions with solid boundaries. This was accounted for in the special case of the model problem in section 2.4, but more generally, the method needs to be modified to account for complex geometries.

To account for interaction with boundaries, it is possible to use the method proposed by Hernández-Ortiz *et al.* [39,40], which is compatible with the use of accelerated algorithms such as SPME. In this method, interactions are first calculated in periodic boundary conditions using the standard SPME method, neglecting the presence of the boundaries. The solution obtained for the Laplace and Stokes equations does not satisfy the appropriate boundary conditions, but it can be corrected by means of an auxiliary solution. The difference between the error made on the boundaries by using periodic boundary conditions and te expected values is used as the boundary condition for the auxiliary problem. This auxiliary problem is solved in the domain with-

out the ions or particles using standard techniques for the solution of the Laplace and Stokes equations. Because efficient techniques such as spectral or multigrid methods may be used for obtaining the auxiliary solution, the additional cost is minimal and the overall solution can be obtained in $O(N \log N)$ operations.

Finally, steric interactions between particles can be included using the algorithm specified in section 2.6.

The methods developed in this study are applicable to a wide range of engineering problems involving electrokinetic flow in highly confined geometries.

APPENDIX A

SCALING OF THE GOVERNING EQUATIONS

A.1 Scaling the one-dimensional PNP equations

The one-dimensional Poisson-Nernst-Planck equations governing the problem in section 2.8 are:

$$\frac{\partial c_\pm}{\partial t} = -\frac{\partial}{\partial X}\left(-D\frac{\partial c_\pm}{\partial X} \mp \mu z e c_\pm \frac{\partial \phi}{\partial X}\right)$$
$$-\varepsilon_0 \frac{\partial^2 \phi}{\partial X^2} = ze(c_+ - c_-)$$

with the boundary conditions:

$$-D\frac{\partial c_\pm}{\partial X} \mp \frac{zeD}{kT} c_\pm \frac{\partial \phi}{\partial X} = 0 \qquad X = 0, L$$
$$\phi = V \qquad X = 0, \qquad \phi = 0 \qquad X = L$$

and the initial condition $c_+ = c_- = c_0$ at $t = 0^-$.

We set $\tau = \frac{\lambda_D L}{D} t$, $\boldsymbol{x} = \boldsymbol{X}/L$, $\phi = \frac{kT}{ze}\phi$, where λ_D is the Debye screening length from equation 2.4, and kT/ze is the thermal voltage from before. Further, we define $c = \frac{c_+ - c_-}{2c_0}$ and $\rho = \frac{c_+ - c_-}{2c_0}$.

Nondimensionalizing, we get

$$\frac{\partial c}{\partial \tau} = \frac{\lambda_D}{L}\frac{\partial}{\partial x}\left(\frac{\partial c}{\partial x} + \rho\frac{\partial \phi}{\partial x}\right) \tag{A.1}$$
$$\frac{\partial \rho}{\partial \tau} = \frac{\lambda_D}{L}\frac{\partial}{\partial x}\left(\frac{\partial \rho}{\partial x} + c\frac{\partial \phi}{\partial x}\right) \tag{A.2}$$
$$-\left(\frac{\lambda_D}{L}\right)^2 \frac{\partial^2 \phi}{\partial x^2} = \rho \tag{A.3}$$

and the boundary condition on the potential changes to $\phi = zeV/kT$ on

$x = 0$. Thus there are only two governing parameters, $\frac{\lambda_D}{L}$ and $\frac{zeV}{kT}$.

A.2 Scaling the Langevin and Poisson's equation

In dimensional variables, the relevant form of Poisson's equation with N positively and negatively charged ions is

$$-\varepsilon_0 \nabla^2 \phi = \rho = \sum_n \pm ze\delta(\boldsymbol{X} - \boldsymbol{X}_n) \tag{A.4}$$

where $\delta(\boldsymbol{X} - \boldsymbol{X}_n)$ has units of inverse volume.

The Langevin equation is

$$\mathrm{d}\boldsymbol{X_n} = \mu(\mp ze\boldsymbol{\nabla}\phi)\mathrm{d}t + \sqrt{2\mu kT\mathrm{d}t}\boldsymbol{n} \tag{A.5}$$

The same scaling as in appendix A.1 is applied to the above equations: $\tau = \frac{\lambda_D L}{D}t$, $\boldsymbol{x} = \boldsymbol{X}/L$, $\phi = \frac{kT}{ze}\phi$, and we define $c_o = N/L^3$

Carrying out the nondimensionalization, Poisson's equation reduces to:

$$\begin{aligned}
&-\varepsilon_0 \frac{kT}{zeL^2}\nabla^2\phi = \sum_n \pm ze\frac{1}{L^3}\delta^*(\boldsymbol{x} - \boldsymbol{x}_n) \\
\implies &-\frac{\varepsilon_0 kT}{2z^2e^2c_0L^2}\nabla^2\phi = \frac{1}{2N}\sum_n \pm\delta^*(\boldsymbol{x} - \boldsymbol{x}_n) \\
\implies &-\left(\frac{\lambda_D}{L}\right)^2\nabla^2\phi = \frac{1}{2N}\sum_n \pm\delta^*(\boldsymbol{x} - \boldsymbol{x}_n)
\end{aligned}$$

The Langevin equation (A.5) becomes

$$\begin{aligned}
L\mathrm{d}\boldsymbol{x}_n &= \frac{D}{kT}(\pm ze)\frac{kT}{zeL}\boldsymbol{\nabla}\phi\frac{\lambda_D L}{D}\mathrm{d}\tau + \sqrt{2D\frac{\lambda_D L}{D}\mathrm{d}\tau}\boldsymbol{n} \\
\implies \mathrm{d}\boldsymbol{x}_n &= \mp(\frac{\lambda_D}{L})\boldsymbol{\nabla}\phi\mathrm{d}\tau + \sqrt{2\frac{\lambda_D}{L}\mathrm{d}\tau}\boldsymbol{n}
\end{aligned}$$

Where the same boundary conditions as in section A.1 apply. As before, the only free parameters are $\frac{\lambda_D}{L}$ and the boundary condition $\frac{zeV}{kT}$.

REFERENCES

[1] T. Squires and S. Quake, "Microfluidics: Fluid physics at the nanoliter scale," *Rev. Modern Phys.*, vol. 77, pp. 977–1026, 2005.

[2] H. A. Stone and S. Kim, "Microfluidics: Basic issues, applications and challenges," *AIChE J.*, vol. 47, pp. 1250–1254, 2001.

[3] H. A. Stone, A. D. Stroock, and A. Adjari, "Engineering flows in small devices: Microfluidics toward lab-on-a-chip." *Annu. Rev. Fluid Mech.*, vol. 36, pp. 381–411, 2004.

[4] C.-F. Chou and et al, "Sorting biomolecules with microdevices," *Electrophoresis*, vol. 21, pp. 81–90, 2000.

[5] D. J. Beebe, G. A. Mensing, and G. M. Walker, "Physics and applications of microfluidics in biology." *Annu. Rev. Biomed. Eng.*, vol. 4, pp. 261–268, 2002.

[6] A. L. Paguirigan and D. J. Beebe, "Microfluidics meet cell biology: bridging the gap by validation and application of microscale techniques for cell biological assays." *BioEssays*, vol. 30, pp. 811–821, 2008.

[7] S. Prakash, A. Piruska, E. N. Gatimu, P. Bohn, J. Sweedler, and M. A. Shannon, "Nanofluidics: Systems and applications," *IEEE Sensors, J.*, vol. 8, pp. 441–450, 2008.

[8] X. B. Wang, J. Yang, Y. Huang, J. Vykoukal, F. F. Becker, and P. R. C. Gascoyne, "Cell separation by dielectrophoretic field-flow fractionation," *Anal. Chem.*, vol. 72, pp. 832–839, 2000.

[9] S. Pennarthur, F. Baldessari, J. G. Santiago, M. G. Kattah, J. B. Steinman, and P. J. Utz, "Free-solution oligonucleotide separation in nanoscale channels," *Anal. Chem.*, vol. 79, pp. 8316–8322, 2007.

[10] J. B. H. Tok, F. Y. S. Chuang, M. C. Cao, K. A. Rose, S. S. Pannu, M. Y. Sha, G. Chakarova, S. G. Penn, and G. M. Dougherty, "Metallic striped nanowires as multiplexed immunoassay platforms for pathogen detection," *Angew. Chem. Ed.*, vol. 45, p. 6900, 2006.

[11] A. Groisman, M. Enzelberger, and S. R. Quake, "Microfluidic memory and control devices." *Science*, vol. 300, p. 955, 2003.

[12] A. Groisman and S. R. Quake, "A microfluidic rectifier: anisotropic flow resistance at low reynolds number." *Phys. Rev. Lett.*, vol. 92, p. 094501, 2004.

[13] D. A. Saville, "Electrokinetic effects with small particles," *Ann. Rev. Fluid. Mech.*, vol. 9, pp. 321–337, 1977.

[14] J. Viovy, "Electrophoresis of dna and other polyelectrolytes: Physical mechanisms." *Reviews of Modern Physics*, vol. 72, pp. 813–872, 2000.

[15] J. L. Anderson, "Colloid transport by interfacial forces." *Annu. Rev. Fluid. Mech*, vol. 30, pp. 139–165, 1989.

[16] R. F. Probstein, *Physiochemical Hydrodynamics: An Introduction.* Wiley Interscience, 2003.

[17] M. P. Allen and D. J. Tildesley, *Computer Simulation of Liquids.* Oxford University Press, 1989.

[18] V. G. Levich, *Physiochemical Hydrodynamics.* Prentice-Hall, 1962.

[19] P. C. Hiemenz and R. Rajagopalan, *Principles of Colloid and Surface Chemistry.* Marcel Dekker, 1997.

[20] M. Smoluchowski, *Handbuch der Elektrizität und des Magnetismus.* Barth-Verlag, Leipzig, 1921, vol. Band II.

[21] F. Baldessari and J. G. Santiago, "Electrophoresis in nanochannels: brief review and speculation," *J. Nanobiotech*, vol. 4, p. 12, 2006.

[22] F. Baldessari, "Electrokinetics in nanochannels, part i. electric double layer overlap and channel-to-well equilibrium." *J. Colloid Interface Sci.*, vol. 325, pp. 526–538, 2008.

[23] F. Baldessari, "Electrokinetics in nanochannels, part ii. mobility dependence on ion density and ionic current measurements." *J. Colloid Interface Sci.*, vol. 325, pp. 539–546, 2008.

[24] M. S. Kilic, M. Z. Bazant, and A. Ajdari, "Steric effects in the dynamics of electrolytes at large applied voltages. i. double-layer charging." *Phys. Rev. E*, vol. 75, no. 021502, 2007.

[25] M. S. Kilic, M. Z. Bazant, and A. Ajdari, "Steric effects in the dynamics of electrolytes at large applied voltages. ii. modified poisson-nernst-planck equations." *Phys. Rev. E*, vol. 75, no. 021503, 2007.

[26] I. Borukhov, D. ANdelman, and H. Orland, "Steric effects in electrolytes: A modified poisson-boltzmann equation," *Phys. Rev. Lett.*, vol. 79, pp. 435–438, 1997.

[27] F. J. B, "Electro-osmosis in a nanometer-scale channel studied by atomistic simulations." *J. Chem. Phys.*, vol. 116, pp. 2194–2200, 2002.

[28] R. Qiao and N. R. Aluru, "Ion concentrations and velocity profiles in nanochannel electroosmotic flows." *J. Chem. Phys.*, vol. 118, pp. 4692–4701, 2003.

[29] W. Zhu, S. J. Singer, Z. Zheng, and A. T. Conlisk, "Electro-osmotic flow of a model electrolyte," *Phys. Rev. E*, vol. 73, no. 051203, 2005.

[30] D. Kim and E. Darve, "Molecular dynamics simulation of electro-osmotic flows in rough wall nanochannels," *Phys. Rev. E*, vol. 73, no. 051203, 2006.

[31] D. Kim and E. Darve, "High-ionic-strength electroosmotic flows in uncharged hydrophobic nanochannels." *J. Colloid Interface Sci.*, vol. 330, pp. 194–200, 2009.

[32] J. Lyklema, *Fudamentals of Interface and Colloid Science, Volume I: Fundamentals*. Academic Press, San Diego, CA, 1991.

[33] J. Newman, *Electrochemical Systems*, 2nd ed. Prentice-Hall, 1991.

[34] M. Deserno and C. Holm, "How to mesh up ewald sums. i. a theoretical and numerical comparison of various particle mesh routines," *J. Chem. Phys.*, vol. 109, no. 18, 1998.

[35] D. Saintillan and E. Darve, "A smooth particle-mesh ewald algorithm for stokes suspension simulations: The sedimentation of fibers," *Phys. of Fluids*, vol. 17, no. 03301, 2005.

[36] J. S. Park and D. Saintillan, "Dipolophoresis in large-scale suspensions of ideally polarizable spheres," *J. Fluid Mech.*, vol. 662, pp. 66–90, 2010.

[37] P. Szymczak and A. J. C. Ladd, "Boundary conditions for stochastic solutions of the convection-diffusion equation," *Phys. Review*, vol. 68, no. 036704, 2003.

[38] M. Z. Bazant, K. Thornton, and A. Ajdari, "Diffuse-charge dynamics in electrochemical systems," *Phys. Rev. E*, vol. 70, no. 021506, 2004.

[39] J. P. Hernández-Ortiz, J. J. de Pablo, and M. D. Graham, "$n \log n$ method for hydrodynamic interactions of confined polymer systems: Brownian dynamics." *J. Chem. Phys*, vol. 125, no. 164906, 2006.

[40] J. P. Hernández-Ortiz, J. J. de Pablo, and M. D. Graham, "Fast computation of many particle hydrodynamic and electrostatic interactions in a confined geometry." *Phys. Rev. Lett.*, vol. 98, no. 140602, 2007.